



Nonlinear Aerothermoelastic Analysis of Functionally Graded Rectangular Plates Subjected to Hypersonic Airflow Loadings

V. Khalafi¹, H. Shahverdi^{2*}, S. Noori²

¹ Aerospace Research Institute, Tehran, Iran

² Department of Aerospace Engineering, Amirkabir University of Technology, Tehran, Iran

ABSTRACT: In this study, the aerothermoelastic behavior of functionally graded plates under hypersonic airflow is investigated. The classical plate theory based on both mid-surface and the neutral surface position is used to model the structural treatment. Also, Von Karman strain-displacement relations are utilized to involve the structural nonlinearity. To consider the applied hypersonic aerodynamic loads, nonlinear (third-order) piston theory is employed to model unsteady aerodynamic pressure in hypersonic flow regime. Material properties of the functionally graded panel is assumed to be temperature dependent and altered in the thickness direction according to a simple power law distribution. The generalized differential quadrature method is used to transfer the governing partial differential equation into an ordinary differential equation. The onset of flutter instability, the stability boundaries, and the time response analysis of a functionally graded plate are determined by applying the fourth order Runge-Kutta method. Moreover, the effect of some important parameters such as Mach number, in-plane thermal load, plate thickness ratio, and volume fraction index on the plate aerothermoelastic behavior is examined. Comparison of the obtained results with the available results in the literature confirms the accuracy and reliability of the proposed approach to analyzing aerothermoelastic behavior of functionally graded plates in hypersonic flow.

Review History:

Received: 3 April 2017

Revised: 18 December 2017

Accepted: 31 January 2018

Available Online: 20 February 2018

Keywords:

Differential quadrature method

Aerothermoelastic

Functionally graded material

Hypersonic airflow

1- Introduction

Functionally Graded Materials (FGMs) usually made from a mixture of two materials; their material properties demonstrate a smooth change from one side to another by gradually varying the volume fraction of constituent materials. This gradual transition eliminates interface problems and mitigates thermal stress concentrations. So FGMs have attracted considerable interest as one of the advanced inhomogeneous composite materials in the engineering community, especially in high-temperature applications such as space re-entry vehicles and high-speed aircraft [1]. Panels and outer skins of these vehicles are exposed to combined effects of aerodynamic, thermodynamic, inertial, and elastic forces. Therefore, one of the key factors in the design of their outer skins is the aerothermoelastic considerations. It is observed from the existing literature, the aerothermoelastic behaviors of homogeneous panels have gained considerable attention of the researchers. However, limited works have been focused on the aerothermoelastic response of FGM panels in hypersonic regime. In supersonic/hypersonic regime, the well-known analytical relationship, called piston theory, has been commonly applied to compute aerodynamic pressure loads. Since, in the hypersonic regime, both structural and aerodynamic nonlinearities play an important role in the aeroelastic response of a panel. So linear piston theory is not applicable to such problems, and the nonlinear piston theory (third-order) seems more suitable.

The early study on the aerothermoelastic phenomenon can be traced back to the work of Houbolt [2]. He investigated the aerothermoelastic behavior of aircraft structures in high-speed flight. Bolotin [3] studied the nonlinear flutter of curved

panels and provided a general understanding of all factors contributing to the instability associated with non-conservative problems. Dowell [4] studied the aerothermoelastic stability boundaries and the post-flutter behavior of two and three-dimensional simply supported flat plates. He also collected many types of this research topic in his book [5]. Schaeffer and Heard [6] examined the effect of nonlinear temperature distribution on the aeroelastic response of a simply supported rectangular panel subjected to supersonic flow over one surface. They showed that nonlinear temperature distribution may have a significant effect on flutter instability.

The first interaction of aerodynamic and structural nonlinearities was studied by McIntosh [7, 8] and Eastep and McIntosh [9] in flutter analysis of simply supported two and three-dimensional panels in hypersonic airflow. Xue and Mei [10] investigated nonlinear flutter response of isotropic panels under thermal effects using Finite Element Method (FEM). Also, Xue and Mei [11] studied the nonlinear flutter behavior and the fatigue life of two-dimensional isotropic panels in the frequency domain using FEM. Bein et al. [12] provided the hypersonic flutter of a simply supported, curved shallow orthotropic panel subjected to aerodynamic heating. They showed the ability and fidelity of the third-order piston theory to simulate unsteady aerodynamic pressure in the hypersonic aeroelastic problem. Cheng and Mei [13] studied finite element time domain formulation for panel flutter analysis with thermal effects in hypersonic airflow and discussed how to evolve a chaotic behavior. Pourtakdoust and Fazlzadeh [14] investigated aerothermoelastic analysis of a flat skin panel with wall shear stress effect in high supersonic flow. Their study shows that the domain of transient chaotic instability is diminished when the wall shear stress effect is considered.

Corresponding author, E-mail: h_shahverdi@aut.ac.ir

Culler and McNamara [15] investigated aerothermoelastic response of panel structures in hypersonic flow. They also studied the impact of Fluid-Thermal-Structural coupling on response prediction of hypersonic skin panels [16].

In addition to the performed aeroelastic studies in the field of homogeneous panels, many research works have been carried out on aeroelastic analysis of FGM plates as well as static and dynamic response analyses. Prakash and Ganapathi [17] studied aeroelastic behavior of Functionally Graded (FG) plate in supersonic flow under thermal load using finite element method. Shen [18] analyzed thermal post-buckling of simply supported, shear deformable functionally graded plate using higher-order shear deformation plate theory including thermal effects. Sohn and Kim [19,20] investigated aeroelastic instability and flutter characteristics of functionally graded plate in supersonic flow including thermal effect. and showed the effects of the volume fraction distributions, temperature changes, aerodynamic pressures and the boundary conditions on the panel flutter. Fazelzadeh et al. [21] studied the thermal divergence of FGM flat rectangular panel and geometric parameters such as plate aspect ratio and relative thickness, as well as gradient index on critical temperature and divergence boundaries for uniform and linear temperature distributions. Hosseini et al. [22] studied nonlinear flutter characteristics of functionally graded curved panels under high temperature supersonic flow. Marzocca et al. [23] presented a review of nonlinear aerothermoelasticity of functionally graded panels. Navazi and Haddadpour [24] investigated aeroelastic stability boundaries and nonlinear supersonic flutter behavior of functionally graded plate based on mid-surface formulation and showed that under real flight conditions and using coupled model, the aerodynamic heating is very severe and the type of instability is divergence. Sofiyev [25] investigated buckling of freely-supported FGM truncated and complete conical shells under external pressures in the framework of the shear deformation theory. He also studied the vibration and stability of FGM conical shells under a compressive axial load using Galerkin method [26].

So far, different numerical techniques have been utilized for flutter studies. However, the methods having greater accuracy and much less computational complexity (and effort) are of most interest to researchers. One method that has been widely considered in the recent years is Generalized Differential Quadrature Method (GDQM). In addition to the ease of implementation, GDQM also provides increased efficiency and accuracy by demanding less number of grid points in comparison to another method such as FEM [27]. The DQ method was first presented by Bellman and Casti [28]. The main idea behind DQM is that the derivative of a function with respect to a space variable at a given point is approximated as a weighted linear sum of the function values at all discrete points along the domain of that variable. DQM has been applied to solve various structural elements such as beams, plates and shells. Bert et al. [29] applied the DQM to investigate the static and dynamic response of structures for the first time, and afterward it was improved by Bert and Malik [30]. Also, Bert et al. [31] used DQM for composite plates for the first time and analyzed nonlinear bending of orthotropic rectangular plates. Then, Shu and Richards [32] presented the GDQM to simplify the computation of the weighting coefficients. Shu and Wang [33] applied GDQM for vibration analysis of a rectangular plate with combined

and non-uniform boundary conditions. Fazelzadeh et al. [34] investigated the vibration of a rotating thin walled blade made of functionally graded materials (FGMs) operating under high-temperature supersonic gas flow with DQM. GDQM applied by Tornabene et al. [35] to study the dynamic behavior of FGMs and laminated doubly-curved shells and panels of revolution with a free-form meridian. They verified the accuracy of GDQ method by using commercial programs such as Abaqus, Ansys, Nastran, Straus and Pro/Mechanica. Tornabene et al. [36] applied GDQM to investigate shear strains and stresses in statically deformed FG doubly-curved sandwich shell structures and shells of revolution using the generalized zigzag displacement field and the Carrera Unified Formulation (CUF). Also, Tornabene et al. [37] analyzed doubly-curved laminated composite shells using different kinematic expansions along the three orthogonal directions of the curvilinear shell model using Local Generalized Differential Quadrature method (LGDQM). They showed that the LGDQM compared to the GDQM needs a large number of grid points without losing accuracy and keeping the very good stability features of GDQM. Generalized Differential Quadrature Finite Element Method (GDQFEM) used by Fantuzzi et al. [38] to study the free vibration of moderately thick FGM plates with geometric discontinuities and arbitrarily curved boundaries. At last through 2015, an excellent review of Differential Quadrature Method in a complete way was presented by Tornabene et al. [39].

Shahverdi et al. [40] used GDQM for aerothermoelastic analysis of functionally graded plates and applied the first order piston theory to consider the supersonic aerodynamic loads on the plate. The material properties of the FG panel were assumed to be temperature independent. So the static and dynamic stability margins of simply support FG plates were analyzed for various volume fractions. Shahverdi and Khalafi [41] investigated aero-thermo-elastic behavior of 2-D functionally graded curved panels under simultaneous aerodynamic and thermal loads in hypersonic flow using GDQM.

To the best of the authors' knowledge, GDQM has not been employed in hypersonic panel flutter studies in the literature. In present work, the hypersonic aeroelastic analysis of a FG flat plate in the presence of thermal loading is investigated using GDQM.

In this regard, the governing differential aeroelastic equations of a FG plate are first discretized using GDQM, and then the aerothermoelastic response of the plate is studied by the fourth order Runge-Kutta method. To show the accuracy and reliability of the GDQM, the dynamic stability boundaries of a FG plate are validated with available results presented in the literature. Also, the effects of some important parameters such as Mach number, in-plane thermal load, plate thickness ratio, and volume fraction index on the aerothermoelastic behavior of the FG plate are examined as well as physical neutral surface effect.

2- Formulation

2- 1- Structural model

A rectangular FG panel with length a , width b , and thickness h is considered. The airflow is assumed in the x -direction. The FG panel is assumed to be composed of a ceramic and a metal, and the volume fraction of the functionally graded material varies continuously through the plate thickness

according to a simple power law [17]. Hence:

$$V_m = \left(\frac{z + h/2}{h} \right)^n \tag{1}$$

$$(V_m + V_c = 1) \tag{2}$$

where z is the coordinate in the thickness direction with origin at the plate mid-surface and n is the volume fraction index. Material properties of the functionally graded plate are assumed to vary continuously across the plate thickness according to the simple rule of mixtures as follows [17]:

$$P_{eff} = P_m V_m + P_c V_c \tag{3}$$

$$P_{eff} = (P_c - P_m) \left(\frac{z + h/2}{h} \right)^n + P_m \tag{4}$$

where subscripts c and m refer to ceramic and metal, respectively, and P_{eff} is the effective material properties of the plate corresponding to the modulus of elasticity E , Poisson's ratio ν , density ρ and thermal α coefficient expansion.

However, in high-temperature environments, the temperature dependency of material constituents must be taken into account. Thus, temperature-dependent properties, P , can be obtained as follows [20]:

$$P = P_0 (P_{-1} T^{-1} + 1 + P_1 T^1 + P_2 T^2 + P_3 T^3) \tag{5}$$

where $P_0, P_{-1}, P_1, P_2, P_3$ are constants, and T (in Kelvin) is the environmental temperature.

The Classical Plate Theory (CPT) based on the position of the neutral surface is developed here.

Based on the Classical Plate Theory (CPT) and the physical neutral surface concept, the displacement field of the plate is [42]:

$$\begin{aligned} u(x, y, z, t) &= u_0(x, y, t) - (z - z_0) \frac{\partial w_0(x, y, t)}{\partial x} \\ v(x, y, z, t) &= v_0(x, y, t) - (z - z_0) \frac{\partial w_0(x, y, t)}{\partial y} \end{aligned} \tag{6}$$

$$w(x, y, z, t) = w_0(x, y, t)$$

where u_0 and v_0 are in-plane displacement components, and w_0 is out-of-plane displacement component of neutral surface. z_0 is the distance of the neutral surface from the mid-surface of the plate and can be determined from the following equation as [43]:

$$z_0 = \frac{\int_{-\frac{h}{2}}^{\frac{h}{2}} z E(z) dz}{\int_{-\frac{h}{2}}^{\frac{h}{2}} E(z) dz} \tag{7}$$

The von Karman nonlinear strain-displacement relations, the nonlinear strains are expressed as:

$$\begin{aligned} \begin{Bmatrix} \epsilon_{xx} \\ \epsilon_{yy} \\ \epsilon_{xy} \end{Bmatrix} &= \begin{Bmatrix} u_{0,x} \\ v_{0,y} \\ u_{0,y} + v_{0,x} \end{Bmatrix} + \frac{1}{2} \begin{Bmatrix} w_{0,x}^2 \\ w_{0,y}^2 \\ 2w_{0,x}w_{0,y} \end{Bmatrix} \\ &+ (z - z_0) \begin{Bmatrix} -w_{xx} \\ -w_{yy} \\ -2w_{xy} \end{Bmatrix} \end{aligned} \tag{8}$$

The thermoelastic constitutive equations of the FG panels are:

$$\begin{Bmatrix} \sigma_{xx} \\ \sigma_{yy} \\ \sigma_{xy} \end{Bmatrix} = \begin{bmatrix} Q_{11} & Q_{12} & 0 \\ Q_{12} & Q_{22} & 0 \\ 0 & 0 & Q_{66} \end{bmatrix} \begin{Bmatrix} \epsilon_{xx} - \alpha(z, T) \Delta T(z) \\ \epsilon_{yy} - \alpha(z, T) \Delta T(z) \\ \epsilon_{xy} \end{Bmatrix} \tag{9}$$

$$\Delta T(z) = T(z) - T_0 \tag{10}$$

where T_0 , $T(z)$ and $\alpha(z, T)$ are reference temperature, the temperature distribution in the plate thickness direction and thermal expansion coefficient, respectively. Q_{ij} is the stiffness coefficient matrix and is defined by:

$$\begin{aligned} Q_{11} = Q_{22} &= \frac{E(z)}{1 - \nu(z)^2} \\ Q_{12} &= \frac{\nu(z)E(z)}{1 - \nu(z)^2} \\ Q_{66} &= \frac{E(z)}{2(1 + \nu(z))} \end{aligned} \tag{11}$$

where $E(z)$ is the elastic modulus of a FG panel.

In-plane force resultant and out-of-plate moment resultant are obtained as follows:

$$\begin{Bmatrix} \mathbf{N} \\ \mathbf{M} \end{Bmatrix} = \begin{bmatrix} \mathbf{A} & \mathbf{B} \\ \mathbf{B} & \mathbf{D} \end{bmatrix} \begin{Bmatrix} \{\epsilon^0\} \\ \{k\} \end{Bmatrix} - \begin{Bmatrix} \mathbf{N}^T \\ \mathbf{M}^T \end{Bmatrix} \tag{12}$$

Here, \mathbf{N}^T and \mathbf{M}^T are the thermal in-plane force moment resultant vectors. Thus

$$(\mathbf{N}^T, \mathbf{M}^T) = \int_{-\frac{h}{2}}^{\frac{h}{2}} (1, z) \mathbf{Q} \begin{Bmatrix} \alpha(z) \\ \alpha(z) \\ 0 \end{Bmatrix} \Delta T(z) dz \tag{13}$$

where \mathbf{A} , \mathbf{B} and \mathbf{D} represent extensional, bending-extensional coupling, and bending stiffness matrices, and are given as follows:

$$(A_{ij}, B_{ij}, D_{ij}) = \int_{-\frac{h}{2}}^{\frac{h}{2}} Q_{ij} (1, (z - z_0), (z - z_0)^2) dz \tag{14}$$

Above neutral surface based formulation change to mid-surface formulation when $z_0=0$.

Here, It should be noted that due to Eq. (7), the extension-bending coupling matrix, \mathbf{B} , defined by Eq. (14) always

equals to zero in the neutral surface based formulation.

2- 2- Aerodynamic model

Piston theory represents an inviscid aerodynamic model that has been used extensively in supersonic and hypersonic aeroelasticity. So, piston theory which provides a simple point-function relationship between the unsteady pressure and surface deformation [16], is used in this study. According to the third-order piston theory, the aerodynamic pressure may be expressed as [15]:

$$\Delta p = \frac{2q_\infty}{M} \left[\left(\frac{1}{U_\infty} \frac{\partial w}{\partial t} + \frac{\partial w}{\partial x} \right) + \frac{\gamma+1}{4} M \left(\frac{1}{U_\infty} \frac{\partial w}{\partial t} + \frac{\partial w}{\partial x} \right)^2 \right. \\ \left. + \frac{\gamma+1}{12} M^2 \left(\frac{1}{U_\infty} \frac{\partial w}{\partial t} + \frac{\partial w}{\partial x} \right)^3 \right] \quad (15)$$

where q_∞ , M and U_∞ are the dynamic pressure, Mach number, and the free stream velocity, respectively. It must be noted that the difference between the third-order piston theory and first-order one is the existence of the second and third terms (nonlinear terms) in Eq. 15.

2- 3- Temperature distribution

The temperature distribution on the surface of the plate is assumed to be constant while in the thickness direction it is considered to be variable and may be obtained by solving the one-dimensional Fourier equation of the heat conduction, which is

$$\frac{d}{dz} \left[K(z) \frac{dT}{dz} \right] = 0, \quad \begin{cases} T = T_c & \text{at } z = \frac{h}{2} \\ T = T_m & \text{at } z = -\frac{h}{2} \end{cases} \quad (16)$$

T_m and T_c are the temperatures of the lower and upper surfaces of the panel, and temperature distribution in the plate thickness direction is obtained as follows [44]:

$$T(z) = T_m + (T_c - T_m) \frac{\int_{-\frac{h}{2}}^z \frac{1}{K(z,T)} dz}{\int_{-\frac{h}{2}}^{\frac{h}{2}} \frac{1}{K(z,T)} dz} \quad (17)$$

2- 4- Equations of motion

By using the virtual work principle, the nonlinear governing equations of motion can be obtained. In the absence of surface shearing forces, body moments and inertia forces in the x and y directions, the aeroelastic equations of a FG plate are [31]:

$$\begin{aligned} N_{xx,x} + N_{xy,y} &= 0 \\ N_{xy,x} + N_{yy,y} &= 0 \\ M_{xx,xx} + 2M_{xy,xy} + M_{yy,yy} + N_{xx} \frac{\partial^2 w}{\partial x^2} \\ + 2N_{xy} \frac{\partial^2 w}{\partial x \partial y} + N_{yy} \frac{\partial^2 w}{\partial y^2} + \Delta p_\infty &= I_0 \ddot{w} \end{aligned} \quad (18)$$

where,

$$I_0 = \int_{-h/2}^{h/2} \rho(z) dz \quad (19)$$

By incorporating Eqs. (9) and (12) into Eq. (18), the equations of motion are obtained as follows:

$$\begin{aligned} A_{11} \frac{\partial \varepsilon_{xx}}{\partial x} + A_{12} \frac{\partial \varepsilon_{yy}}{\partial x} + B_{11} \frac{\partial k_{xx}}{\partial x} \\ + B_{12} \frac{\partial k_{yy}}{\partial x} + A_{66} \frac{\partial \varepsilon_{xy}}{\partial y} + B_{66} \frac{\partial k_{xy}}{\partial y} &= 0 \end{aligned} \quad (20)$$

$$\begin{aligned} A_{12} \frac{\partial \varepsilon_{xx}}{\partial y} + A_{22} \frac{\partial \varepsilon_{yy}}{\partial y} + B_{12} \frac{\partial k_{xx}}{\partial y} \\ + B_{22} \frac{\partial k_{yy}}{\partial y} + A_{66} \frac{\partial \varepsilon_{xy}}{\partial x} + B_{66} \frac{\partial k_{xy}}{\partial x} &= 0 \end{aligned} \quad (21)$$

$$\begin{aligned} B_{11} \frac{\partial^2 \varepsilon_{xx}}{\partial x^2} + B_{12} \frac{\partial^2 \varepsilon_{yy}}{\partial x^2} + D_{11} \frac{\partial^2 k_{xx}}{\partial x^2} + D_{12} \frac{\partial^2 k_{yy}}{\partial x^2} \\ + B_{12} \frac{\partial^2 \varepsilon_{xx}}{\partial y^2} + B_{22} \frac{\partial^2 \varepsilon_{yy}}{\partial y^2} + D_{12} \frac{\partial^2 k_{xx}}{\partial y^2} + D_{22} \frac{\partial^2 k_{yy}}{\partial y^2} \\ + 2B_{66} \frac{\partial^2 \varepsilon_{xy}}{\partial x \partial y} + 2D_{66} \frac{\partial^2 k_{xy}}{\partial x \partial y} + N_{xx} \frac{\partial^2 w}{\partial x^2} \\ + 2N_{xy} \frac{\partial^2 w}{\partial x \partial y} + N_{yy} \frac{\partial^2 w}{\partial y^2} + \Delta p_\infty = I_0 \ddot{w} \end{aligned} \quad (22)$$

With differentiating from Eqs. (20) and (21) with respect to the variables of x and y , respectively, and adding the resulted equation, we will have:

$$\begin{aligned} A_{11} \frac{\partial^2 \varepsilon_{xx}}{\partial x^2} + A_{12} \frac{\partial^2 \varepsilon_{yy}}{\partial x^2} + B_{11} \frac{\partial^2 k_{xx}}{\partial x^2} + B_{12} \frac{\partial^2 k_{yy}}{\partial x^2} \\ + A_{66} \frac{\partial^2 \varepsilon_{xy}}{\partial x \partial y} + B_{66} \frac{\partial^2 k_{xy}}{\partial x \partial y} + A_{12} \frac{\partial^2 \varepsilon_{xx}}{\partial y^2} + A_{22} \frac{\partial^2 \varepsilon_{yy}}{\partial y^2} \\ + B_{12} \frac{\partial^2 k_{xx}}{\partial y^2} + B_{22} \frac{\partial^2 k_{yy}}{\partial y^2} + A_{66} \frac{\partial^2 \varepsilon_{xy}}{\partial x \partial y} + B_{66} \frac{\partial^2 k_{xy}}{\partial x \partial y} &= 0 \end{aligned} \quad (23)$$

By multiplying to Eq. (22) and to Eq. (23) and collected them together after some mathematical manipulations, the following equation is obtained:

$$\begin{aligned} & \frac{(D_{11}A_{11} - B_{11}^2)}{A_{11}} \frac{\partial^2 k_{xx}}{\partial x^2} + \nu \frac{(D_{11}A_{11} - B_{11}^2)}{A_{11}} \frac{\partial^2 k_{yy}}{\partial x^2} \\ & + \nu \frac{(D_{11}A_{11} - B_{11}^2)}{A_{11}} \frac{\partial^2 k_{xx}}{\partial y^2} + \frac{(D_{11}A_{11} - B_{11}^2)}{A_{11}} \frac{\partial^2 k_{yy}}{\partial y^2} \\ & + 2 \left(\frac{1-\nu}{2} \right) \frac{(D_{11}A_{11} - B_{11}^2)}{A_{11}} \frac{\partial^2 k_{xy}}{\partial x \partial y} + N_{xx} \frac{\partial^2 w}{\partial x^2} \\ & + 2N_{xy} \frac{\partial^2 w}{\partial x \partial y} + N_{yy} \frac{\partial^2 w}{\partial y^2} + \Delta p_\infty = I_0 \ddot{w} \end{aligned} \quad (24)$$

The above equation can be written as:

$$\begin{aligned} & D_{eq} \left(\frac{\partial^4 w}{\partial x^4} + 2 \frac{\partial^4 w}{\partial x^2 \partial y^2} + \frac{\partial^4 w}{\partial y^4} \right) + N_{xx} \frac{\partial^2 w}{\partial x^2} + 2N_{xy} \frac{\partial^2 w}{\partial x \partial y} \\ & + N_{yy} \frac{\partial^2 w}{\partial y^2} + \Delta p_\infty + I_0 \ddot{w} = 0 \end{aligned} \quad (25)$$

where,

$$D_{eq} = \frac{D_{11}A_{11} - B_{11}^2}{A_{11}} \quad (26)$$

In this paper, the plate is considered to be simply supported along all edges and, therefore, the in-plane displacement components $\partial u/\partial x$, $\partial v/\partial y$, $\partial u/\partial y$, $\partial v/\partial x$ are equal to zero and, based on this assumption, in-plane force resultants can be modified as (see[5, 42]):

$$\begin{aligned} N_{xx} &= \int_0^b \int_0^a \left(A_{11} \frac{1}{2} \left(\frac{\partial w}{\partial x} \right)^2 + A_{12} \frac{1}{2} \left(\frac{\partial w}{\partial y} \right)^2 - B_{11} \frac{\partial^2 w}{\partial x^2} - B_{12} \frac{\partial^2 w}{\partial x^2 \partial y} \right) dx dy - N_{xx}^r \\ N_{yy} &= \int_0^b \int_0^a \left(A_{12} \frac{1}{2} \left(\frac{\partial w}{\partial x} \right)^2 + A_{22} \frac{1}{2} \left(\frac{\partial w}{\partial y} \right)^2 - B_{12} \frac{\partial^2 w}{\partial x^2} - B_{22} \frac{\partial^2 w}{\partial x^2 \partial y} \right) dx dy - N_{yy}^r \\ N_{xy} &= \int_0^b \int_0^a \left(A_{66} \frac{\partial w}{\partial x} \frac{\partial w}{\partial y} - 2B_{66} \frac{\partial^2 w}{\partial x \partial y} \right) dx dy \end{aligned} \quad (27)$$

By substituting Eqs. (15) and (27) into Eq. (25), the aerothermoelastic equation is obtained as:

$$\begin{aligned} & D_{eq} \left(\frac{\partial^4 w}{\partial x^4} + 2 \frac{\partial^4 w}{\partial x^2 \partial y^2} + \frac{\partial^4 w}{\partial y^4} \right) \\ & + \left[\int_0^b \int_0^a \left(A_{11} \frac{1}{2} \left(\frac{\partial w}{\partial x} \right)^2 + A_{12} \frac{1}{2} \left(\frac{\partial w}{\partial y} \right)^2 - B_{11} \frac{\partial^2 w}{\partial x^2} - B_{12} \frac{\partial^2 w}{\partial x^2 \partial y} \right) dx dy \right] \frac{\partial^2 w}{\partial x^2} \\ & + 2 \left[\int_0^b \int_0^a \left(A_{66} \frac{\partial w}{\partial x} \frac{\partial w}{\partial y} - 2B_{66} \frac{\partial^2 w}{\partial x \partial y} \right) dx dy \right] \frac{\partial^2 w}{\partial x \partial y} \\ & + \left[\int_0^b \int_0^a \left(A_{12} \frac{1}{2} \left(\frac{\partial w}{\partial x} \right)^2 + A_{22} \frac{1}{2} \left(\frac{\partial w}{\partial y} \right)^2 - B_{12} \frac{\partial^2 w}{\partial x^2} - B_{22} \frac{\partial^2 w}{\partial y^2} \right) dx dy \right] \frac{\partial^2 w}{\partial y^2} \\ & - N_{xx}^r \frac{\partial^2 w}{\partial x^2} - N_{yy}^r \frac{\partial^2 w}{\partial y^2} \\ & + \frac{2q_\infty}{M_\infty} \left[\left(\frac{1}{U_\infty} \frac{\partial w}{\partial t} + \frac{\partial w}{\partial x} \right) + \frac{\gamma+1}{4} M_\infty \left(\frac{1}{U_\infty} \frac{\partial w}{\partial t} + \frac{\partial w}{\partial x} \right)^2 \right] \\ & + \frac{M_\infty}{12} \left[\frac{\gamma+1}{12} M_\infty^2 \left(\frac{1}{U_\infty} \frac{\partial w}{\partial t} + \frac{\partial w}{\partial x} \right)^3 \right] \end{aligned} \quad (28)$$

The following sets of dimensionless parameters are defined as follows:

$$\begin{aligned} W &= \frac{w}{h} & \zeta &= \frac{x}{a} \\ \eta &= \frac{y}{b} & \lambda &= \frac{2q_\infty a^3}{MD_m} \\ \mu &= \frac{\rho_\infty a}{\rho_m h} & \tau &= t \left(\frac{D_m}{\rho_m h a^4} \right)^{1/2} \\ R_x &= \frac{N_{xx}^r a^2}{D_m} & R_y &= \frac{N_{yy}^r b^2}{D_m} \end{aligned} \quad (29)$$

By incorporating the above parameters in Eq. (28), the non-dimensional form of aeroelastic equations can be obtained.

$$\begin{aligned} & \frac{I_0}{\rho_m h} \frac{\partial^3 W}{\partial \tau^2} + \frac{D_{eq}}{D_m} \left(\frac{\partial^4 W}{\partial \zeta^4} + 2 \left(\frac{a}{b} \right)^2 \frac{\partial^3 W}{\partial \zeta^2 \partial \eta^2} + \left(\frac{a}{b} \right)^4 \frac{\partial^2 W}{\partial \eta^4} \right) \\ & + \left[\int_0^1 \int_0^1 \left(A_{11} \frac{abh^2}{2D_m} \left(\frac{\partial W}{\partial \zeta} \right)^2 + A_{12} \frac{a^3 h^2}{2bD_m} \left(\frac{\partial W}{\partial \eta} \right)^2 \right) d\zeta d\eta \right] \frac{\partial^3 W}{\partial \zeta^2} \\ & + 2 \left[\int_0^1 \int_0^1 \left(A_{66} \frac{a^3 h^2}{bD_m} \frac{\partial W}{\partial \zeta} \frac{\partial W}{\partial \eta} - 2B_{66} \frac{a^3 h}{bD_m} \frac{\partial^2 W}{\partial \zeta \partial \eta} \right) d\zeta d\eta \right] \frac{\partial^3 W}{\partial \zeta \partial \eta} \\ & + \left[\int_0^1 \int_0^1 \left(A_{12} \frac{a^3 h^2}{2bD_m} \left(\frac{\partial W}{\partial \zeta} \right)^2 + A_{22} \frac{abh^2}{2D_m} \left(\frac{\partial W}{\partial \eta} \right)^2 \right) d\zeta d\eta \right] \frac{\partial^3 W}{\partial \eta^2} \quad (30) \\ & - R_x \frac{\partial^3 W}{\partial \zeta^2} - R_y \left(\frac{a}{b} \right)^2 \frac{\partial^3 W}{\partial \eta^2} - R_x \frac{\partial^3 W}{\partial \zeta^2} \\ & - R_y \left(\frac{a}{b} \right)^4 \frac{\partial^3 W}{\partial \eta^2} + \lambda \left(\frac{\partial W}{\partial \zeta} + \left(\frac{\mu}{\lambda M} \right)^{1/2} \frac{\partial W}{\partial \tau} \right) \\ & + \lambda \left(M \frac{h}{a} \right) \frac{\gamma+1}{4} \left(\frac{\partial W}{\partial \zeta} + \left(\frac{\mu}{\lambda M} \right)^{1/2} \frac{\partial W}{\partial \tau} \right)^2 \\ & + \lambda \left(M \frac{h}{a} \right)^2 \frac{\gamma+1}{12} \left(\frac{\partial W}{\partial \zeta} + \left(\frac{\mu}{\lambda M} \right)^{1/2} \frac{\partial W}{\partial \tau} \right)^3 = 0 \end{aligned}$$

3- Procedure of Applying GDQM

In this section, the governing aeroelastic equation is discretized by using the GDQM. This method implies that the *r*th-order derivative of a function *W*, at a point $s = s_i$, with *N* discrete points can be estimated by

$$\frac{\partial^r W}{\partial s^r} \Big|_{s=s_i} = \sum_{j=1}^N A_{ij}^{(r)s} W_j \quad (31)$$

The coefficient $A_{ij}^{(r)s}$ represents the weights ($j=1,2,\dots,N$) at the point *i*. The method for constructing the weighted coefficients can be found in Chang Shu [39].

The DQ method may also be used for linear combinations of partial derivatives and integrals [45] as follows:

$$\frac{\partial^{(r+s)} W}{\partial x^r \partial y^s} = \sum_{k=1}^N \sum_{l=1}^M A_{ik}^{(r)x} A_{jl}^{(s)y} W_{kl} \quad (32)$$

$$\int_0^a \int_0^b W(x,y) dx dy = \sum_{k=1}^N \sum_{l=1}^M c_k c_l W_{kl} \quad (33)$$

where c_l, c_k are weighting coefficients of the one-dimensional integral in the *x* and *y* directions respectively, and are given by [45]

$$c_k = H_{jk}^{I(x)} - H_{ik}^{I(x)} = \int_0^a r_k(x) dx \quad (34)$$

$$c_i = H_{jl}^{I(y)} - H_{il}^{I(y)} = \int_0^b r_i(y) dy \quad (35)$$

where

$$H^{I(x)} = (A^{(1)x})^{-1}, H^{I(y)} = (A^{(1)y})^{-1} \quad (36)$$

In the above equations $r_k(x)$ and $r_l(y)$ are the Lagrange interpolated polynomials. By using the GDQM, the discretized form of the governing equations (Eq. (30)) can be written as:

$$\begin{aligned} & \frac{I_0}{\rho_m h} \ddot{W} + \frac{D_{eq}}{D_m} \left(2 \left(\frac{a}{b} \right)^2 \sum_{k=1}^N \sum_{l=1}^M A_{ik1}^{(2)} A_{jk2}^{(2)} W_{k1k2} \right. \\ & \left. + \left(\frac{a}{b} \right)^4 \sum_{k=2=1}^M A_{jk2}^{(4)} W_{ik2} \right) \\ & + A_{11} \frac{abh^2}{2D_m} \sum_{k,l,m,n=1}^N \sum_{p=1}^M c_k c_p A_{kn}^{(1)x} A_{pm}^{(1)x} A_{il}^{(2)x} W_{kn} W_{pm} W_{lj} \\ & + A_{12} \frac{a^3 h^2}{2bD_m} \sum_{k,l=1}^N \sum_{p,q,s=1}^M c_k c_p A_{kq}^{(1)y} A_{ps}^{(1)y} A_{il}^{(2)x} W_{kq} W_{ps} W_{lj} \\ & - B_{11} \frac{abh}{D_m} \sum_{k,l,n=1}^N \sum_{p=1}^M c_k c_p A_{kn}^{(2)x} A_{il}^{(2)x} W_{pn} W_{lj} \\ & - B_{12} \frac{a^3 h}{bD_m} \sum_{k,l=1}^N \sum_{p,q=1}^M c_k c_p A_{pq}^{(2)y} A_{il}^{(2)x} W_{kq} W_{lj} \\ & + 2A_{66} \frac{a^3 h^2}{bD_m} \sum_{k,k,1,n=1}^N \sum_{p,k,2,q=1}^M c_k c_p A_{kn}^{(1)x} A_{pq}^{(1)y} A_{ik1}^{(1)x} A_{jk2}^{(1)y} W_{kn} W_{pq} W_{k k} \\ & - 4B_{66} \frac{a^3 h}{bD_m} \sum_{k,k,1,n=1}^N \sum_{p,k,2,q=1}^M c_k c_p A_{kn}^{(1)x} A_{pq}^{(1)y} A_{ik1}^{(1)x} A_{jk2}^{(1)y} W_{nq} W_{k1k2} \\ & + A_{12} \frac{a^3 h^2}{2bD_m} \sum_{k=1}^N \sum_{p,q,l,s=1}^M c_k c_p A_{ks}^{(1)x} A_{pt}^{(1)x} A_{jq}^{(2)y} W_{ks} W_{pt} W_{iq} \\ & + A_{22} \frac{abh^2}{2D_m} \sum_{k,m,n=1}^N \sum_{p,q=1}^M c_k c_p A_{pm}^{(1)y} A_{kn}^{(1)y} A_{jq}^{(2)y} W_{pm} W_{kn} W_{iq} \\ & - B_{12} \frac{a^3 h}{bD_m} \sum_{k=1}^N \sum_{p,q,l=1}^M c_k c_p A_{pt}^{(2)x} A_{jq}^{(2)y} W_{kl} W_{iq} \\ & - B_{22} \frac{abh}{D_m} \sum_{k,n=1}^N \sum_{p,q=1}^M c_k c_p A_{kn}^{(2)y} A_{jq}^{(2)y} W_{pn} W_{iq} \\ & - R_x \sum_{k=1}^N A_{ik1}^{(2)x} W_{k1j} - R_y \left(\frac{a}{b} \right)^4 \sum_{k=2=1}^M A_{jk2}^{(2)y} W_{ik2} \\ & + \lambda \left(\sum_{k=1}^N A_{ik1}^{(1)x} W_{k1j} + \left(\frac{\mu}{\lambda M} \right)^{1/2} \dot{W} \right) \\ & + \lambda \left(M \frac{h}{a} \right) \frac{\gamma+1}{4} \left(\sum_{k=1}^N A_{ik1}^{(1)x} W_{k1j} + \left(\frac{\mu}{\lambda M} \right)^{1/2} \dot{W} \right)^2 \\ & + \lambda \left(M \frac{h}{a} \right)^2 \frac{\gamma+1}{12} \left(\sum_{k=1}^N A_{ik1}^{(1)x} W_{k1j} + \left(\frac{\mu}{\lambda M} \right)^{1/2} \dot{W} \right)^3 = 0 \end{aligned} \quad (37)$$

for $i, k, k, m, n, k 1 = 1, 2, \dots, N$
 $j, p, q, s, t, k 2 = 1, 2, \dots, M$

Also, the assumed boundary conditions may be written as follow: M

$$\begin{aligned} w(0, y, t) = 0, & \quad M_x(0, y, t) = 0 \\ w(a, y, t) = 0, & \quad M_x(a, y, t) = 0 \\ w(x, 0, t) = 0, & \quad M_y(x, 0, t) = 0 \\ w(x, b, t) = 0, & \quad M_y(x, b, t) = 0 \end{aligned} \tag{38}$$

By incorporating the boundary conditions into Eq. (37) and doing some manipulations, the final aerothermoelastic equation of a FG plate can be drawn as:

$$\begin{aligned} & \left(\frac{I_0}{\rho_m h} \ddot{W} + \frac{D_{eq}}{D_m} \left(\sum_{k=3}^{N-2} C_1 W_{kj} + \left(\frac{a}{b}\right)^4 \sum_{k=3}^{M-2} C_3 W_{ik} \right) \right. \\ & \left. + 2 \left(\frac{a}{b}\right)^2 \sum_{k=1}^{N-2} \sum_{l=3}^{M-2} C_2 W_{k1k2} \right) \\ & + A_{11} \frac{abh^2}{2D_m} \sum_{k,l,m,n=3}^{N-2} \sum_{p=3}^{M-2} C_4 W_{kn} W_{pm} W_{lj} \\ & + A_{12} \frac{a^3 h^2}{2bD_m} \sum_{k,l=3}^{N-2} \sum_{m,n,p=3}^{M-2} C_5 W_{kp} W_{mn} W_{lj} \\ & - B_{11} \frac{abh}{D_m} \sum_{k,l,n=3}^{N-2} \sum_{p=3}^{M-2} C_6 W_{pn} W_{lj} \\ & - B_{12} \frac{a^3 h}{bD_m} \sum_{k,l=3}^{N-2} \sum_{p,q=3}^{M-2} C_7 W_{kq} W_{lj} \\ & + 2A_{66} \frac{a^3 h^2}{bD_m} \sum_{k,k_1,n=3}^{N-2} \sum_{p,k_2,q=3}^{M-2} C_8 W_{kn} W_{pq} W_{k_1k_2} \\ & - 4B_{66} \frac{a^3 h}{bD_m} \sum_{k,k_1,n=3}^{N-2} \sum_{p,k_2,q=3}^{M-2} C_9 W_{nq} W_{k_1k_2} \\ & + A_{12} \frac{a^3 h^2}{2bD_m} \sum_{k=3}^{N-2} \sum_{p,q,l,s=3}^{M-2} C_{10} W_{ks} W_{pl} W_{iq} \\ & + A_{22} \frac{abh^2}{2D_m} \sum_{k,m,n=3}^{N-2} \sum_{p,q=3}^{M-2} C_{11} W_{pm} W_{kn} W_{iq} \\ & - B_{12} \frac{a^3 h}{bD_m} \sum_{k=3}^{N-2} \sum_{p,q,l=3}^{M-2} C_{12} W_{kl} W_{iq} \\ & - B_{22} \frac{abh}{D_m} \sum_{k,n=3}^{N-2} \sum_{p,q=3}^{M-2} C_{13} W_{pn} W_{iq} \\ & - R_x \sum_{k=3}^{N-2} C_{14} W_{kj} \\ & - R_y \left(\frac{a}{b}\right)^4 \sum_{k=3}^{M-2} C_{15} W_{ik} + \lambda \left(\sum_{k=1}^N C_{16} W_{k1j} + \left(\frac{\mu}{\lambda M}\right)^{1/2} \dot{W} \right) \\ & + \lambda \left(M \frac{h}{a} \right) \frac{\gamma+1}{4} \left(\sum_{k=1}^N C_{16} W_{k1j} + \left(\frac{\mu}{\lambda M}\right)^{1/2} \dot{W} \right)^2 \\ & + \lambda \left(M \frac{h}{a} \right) \frac{\gamma+1}{12} \left(\sum_{k=1}^N C_{16} W_{k1j} + \left(\frac{\mu}{\lambda M}\right)^{1/2} \dot{W} \right)^3 = 0 \end{aligned} \tag{39}$$

where C_1 to C_{16} are defined in Appendix A.

4- Results and Discussion

In this section, the aeroelastic behaviors of FG plates are calculated to investigate the validity of the GDQM for determining flutter characteristics. In this regard, a simply-supported square ($a/b=1$) functionally graded flat plate made of a combination of metal (SUS304) and ceramic (Si3N3) is considered as a test case. The material properties are listed in Tables 1 [24].

In order to obtain the flutter instability, the governing aerothermoelastic equation (Eq. (39)) is utilized by considering 11×11 sample points in the computational domain. However, after some investigations, it was found that the present nonlinear analysis is extremely sensitive to the sampling point distribution. Thus, Chebyshev-Gauss-Lobatto distribution is not a right choice for this type of problems, but the suggested distribution by Tomasiello [46] can be used as an alternative choice. Then, the resulting ordinary differential equations are solved via the 4th order Runge-Kutta method. First of all, the limit cycle amplitudes of an FGM square plate for various dynamic pressures at the specified location on the plate surface ($\xi=x/a=0.75$ and $\eta=y/a=0.5$) based on neutral surface formulation are computed and depicted in Fig. 1. As it is evident, the GDQM results are in satisfactory agreement with those presented in Navazi [24], which use mid-surface based formulation and time integration method.

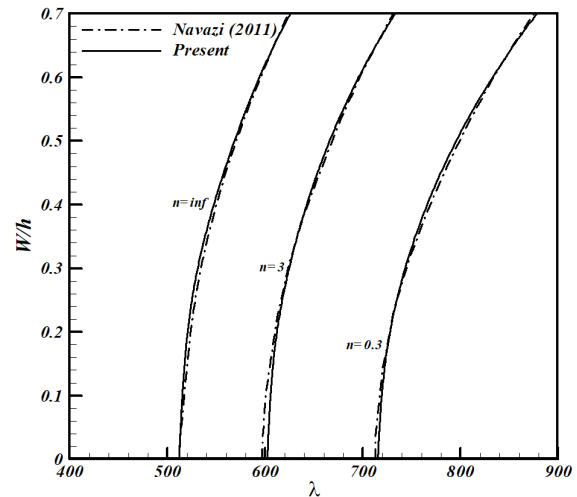


Fig. 1. LCO amplitudes of an FG square plate

The limit cycle amplitudes of an FGM plate ($a/b=1$, $a/h=100$) at $M=5$ for various volume fraction indexes are shown in Fig. 2.

The variation of limit cycle deflections (w/h) with respect to non-dimensional dynamic pressure, λ , is presented in this figure for both neutral surface based and mid-surface based formulation. It can be concluded that the results of two aforementioned reference surfaces are very close together for thin plate theory applications. It is found that a slight increase in λ can dramatically increase in w/h . Also, the critical pressure will be decreased by increasing the volume fraction index (n).

Next, the critical pressures, in which flutter occurs, for the FG panel with various volume fractions and two different values of T_m have been tabulated in Table 2. It is clear that increasing the Mach number has little effect on the critical pressures. On the other hand, the increase of volume fraction index

Table 1. Temperature dependent thermoelastic material properties

Material	P	P_0	P_{-1}	P_1	P_2	P_3
SUS304	$E(\text{Pa})$	201.04E9	0	3.079E-4	-6.534E-7	0
	$\alpha(1/\text{K})$	1.23E-5	0	8.086E-4	0	0
Si3N3	$E(\text{Pa})$	348.43E9	0	-3.07E-4	2.16E-7	-8.946E-11
	$\alpha(1/\text{K})$	5.8723E-6	0	9.095E-4	0	0

Table 2. Critical non-dimensional dynamic pressure

Temperature changes of the surfaces	n	λ_{cr}	λ_{cr}	λ_{cr}	λ_{cr}
		Linear piston theory ($\mu/M=0.01$)	Nonlinear piston theory ($M=2$)	Nonlinear piston theory ($M=5$)	Nonlinear piston theory ($M=8$)
$T_m=300$ $T_c=320$	$n=0.0$	629.75	629.51	629.22	629.20
	$n=0.5$	542.23	541.83	541.38	541.06
	$n=1$	462.16	461.86	461.24	461.09
	$n=5$	409.96	409.78	409.22	408.98
	$n=\infty$	308.04	307.95	307.58	307.48
$T_m=310$ $T_c=320$	$n=0.0$	553.46	553.08	552.34	552.12
	$n=0.5$	452.20	452.04	451.58	451.46
	$n=1$	365.03	364.89	364.63	364.49
	$n=5$	311.60	311.52	311.24	311.17
	$n=\infty$	214.49	214.46	214.38	213.96

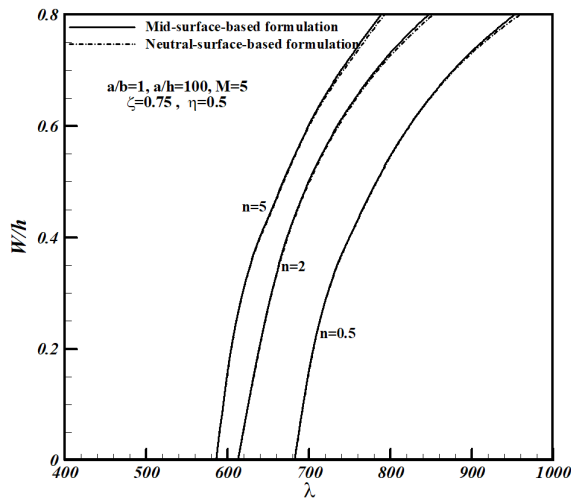


Fig. 2. LCO amplitudes of an FG square plate for both mid-surface and neutral surface based formulation

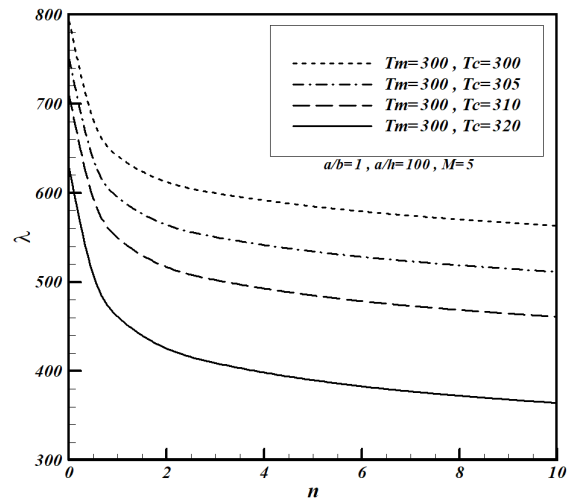


Fig. 3. Effect of surface temperature (T_c) on the critical dynamic pressure of a FG plate ($M=5$)

and lower surface temperature of the plate (T_m) for the same volume fractions leads to reduced critical dynamic pressure. Then, the effects of top surface temperature of the plate (T_c) on critical dynamic pressure are presented in Fig. 3. It can be seen that the critical dynamic pressure increases with decreasing of the top surface temperature of the plate for the same volume fractions. It is clear that critical pressure is greatly decreased up to $n=1$ for any values of T_m and T_c . However, after that value of n the reduction rate of critical pressure decreases in linear fashion. Also, the effects of the thickness ratios (a/h) on critical dynamic pressure are presented in Fig. 4. As the figure shows,

the critical dynamic pressure decreases with increasing the plate thickness ratios (a/h) at the same volume fractions. Moreover, the variation of critical dynamic pressure with respect to thickness ratios (a/h) is more dominant for the case which has a higher value of surface temperature (T_c). The bifurcation diagrams for maximum deflection amplitude of a FG plate ($a/b=1$, $a/h=100$), with $\lambda=500$, versus upper surface temperature, T_c , for two values of n and M , are depicted in Figs. 5 and 6. It is clear that as the volume fraction index (n) increases, the bifurcation point shifts to the left side of this figure and the chaotic motion occurs at the lower value of upper surface

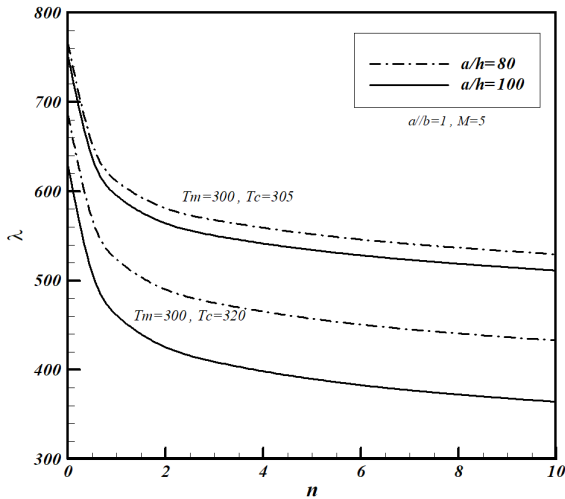
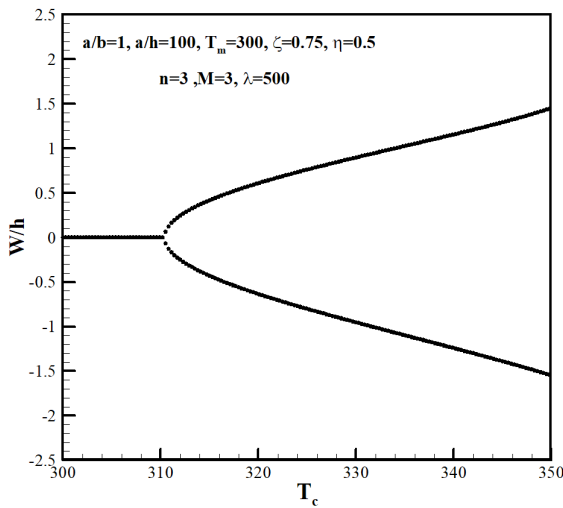
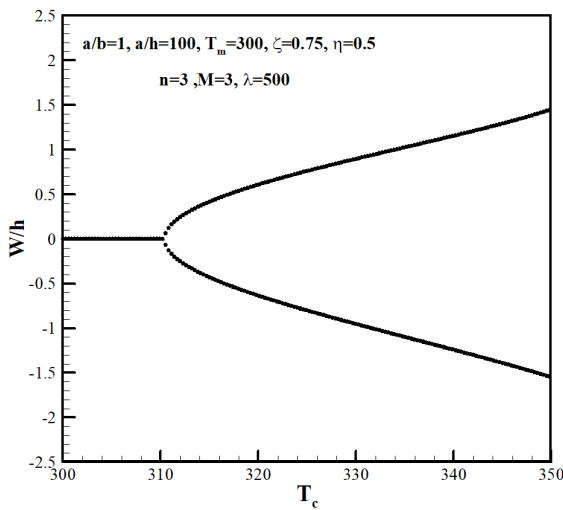


Fig. 4. Effect the plate thickness ratios (a/h) on the critical dynamic pressure of a FG plate ($M=5$)

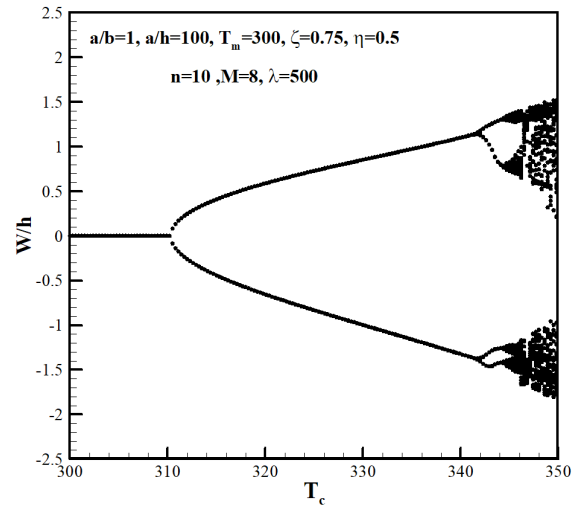


(a)

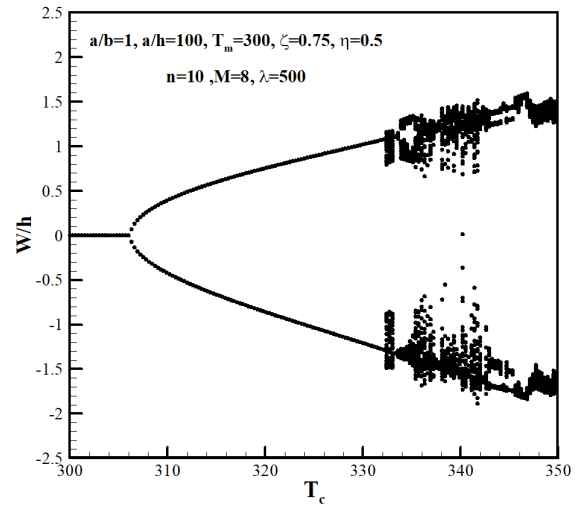


(b)

Fig. 5. Bifurcation diagram of FG plate under increasing T_c , with $\lambda=500$, $M=3$ and $T_m=300$ k. (a) $n=3$, (b) $n=10$



(a)



(b)

Fig. 6. Bifurcation diagram of FG plate under increasing T_c , with $\lambda=500$, $M=8$ and $T_m=300$ k. (a) $n=3$, (b) $n=10$

temperature. On the other hand, when the Mach number increases, the chaotic motion occurs at the lower value of upper surface temperature (T_c).

The effect of using the first and third-order piston theory on the aeroelastic response of the FG plate is shown in Fig. 7. In this figure, the limit cycle amplitude of the FG plate at the aforementioned point ($\zeta=0.75$ and $\eta=0.5$) versus the critical dynamic pressure for various volume fraction indexes is shown. It was found that when the Mach number is set to 2.0, the results of the implementation of the linear and nonlinear piston theory show very little difference. But this difference is greater when Mach number increases toward the hypersonic regime specifically for greater non-dimensional dynamic pressures.

The aerothermoelastic stability margins versus in-plane thermal load for the FG plate for various volume fraction indexes are shown in Fig. 8. It can be seen that as volume fraction index decreases, the critical thermal buckling load, the critical dynamic pressure and the in-plane thermal load, where the chaotic motion begins, all increase. As a result, the bifurcation point shifts to the top right.

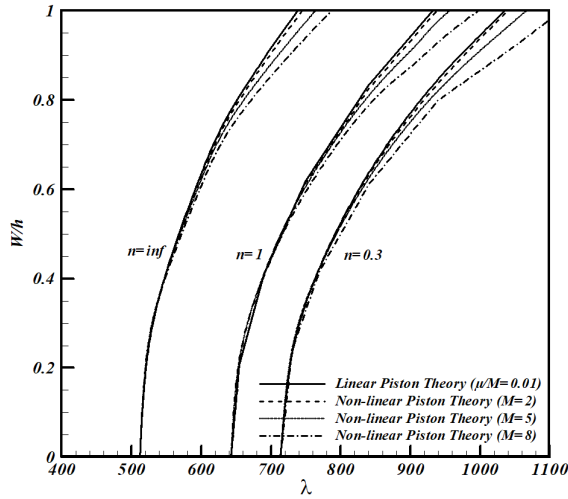


Fig. 7. LCO amplitudes of an FG square plate under different aerodynamic model.

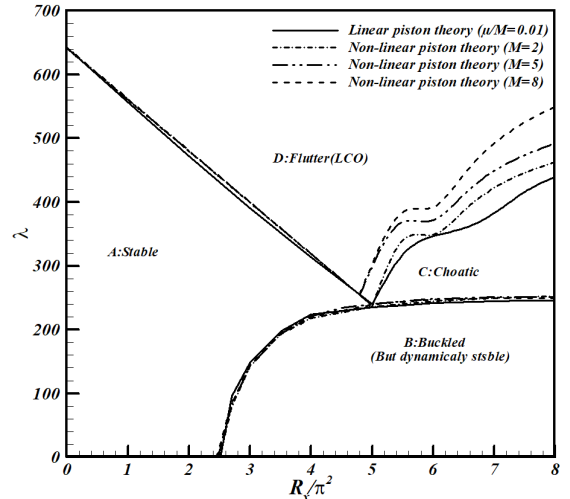


Fig. 9. Stability boundaries of FG plate at various Mach number

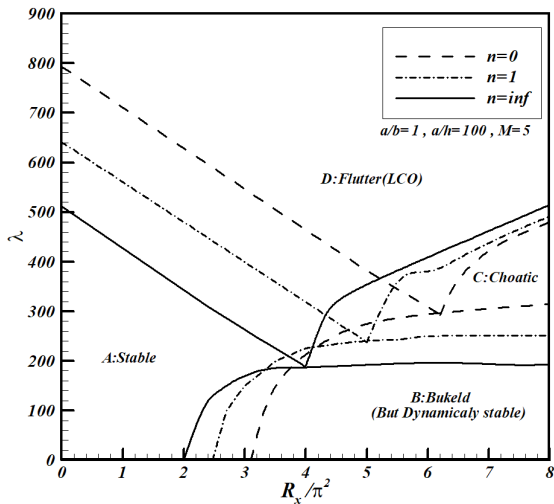
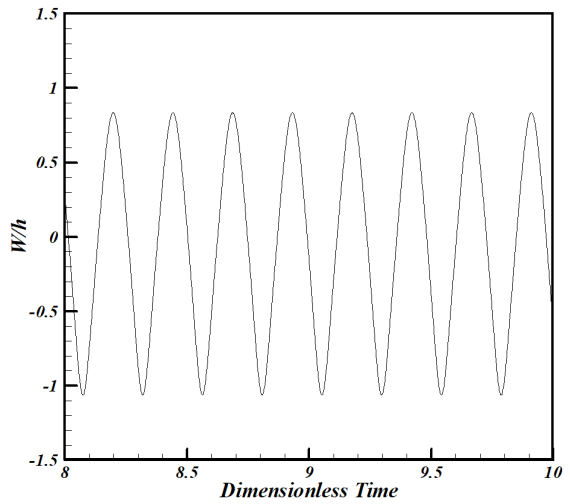
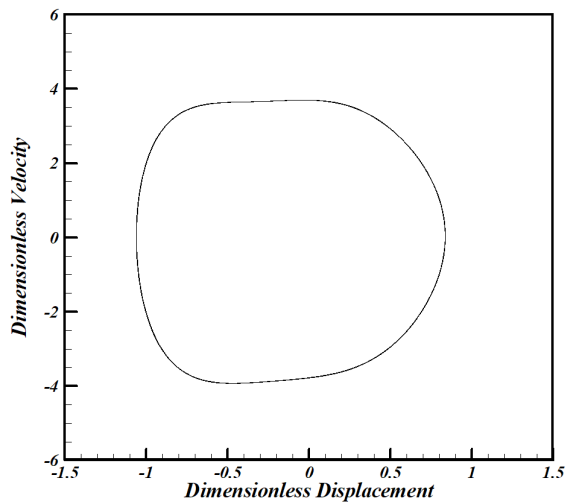


Fig. 8. Stability boundaries of FG plate at various n



(a)

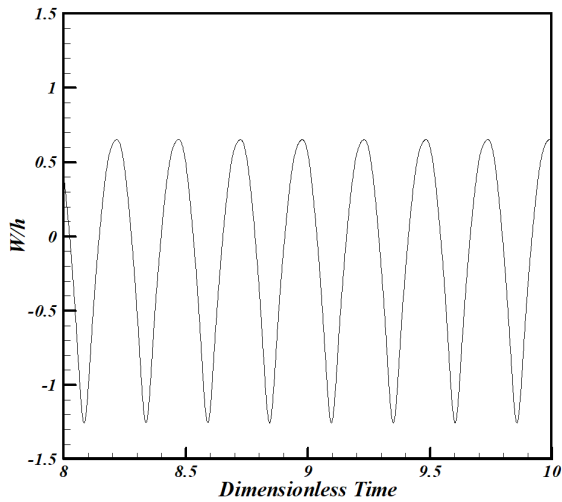


(b)

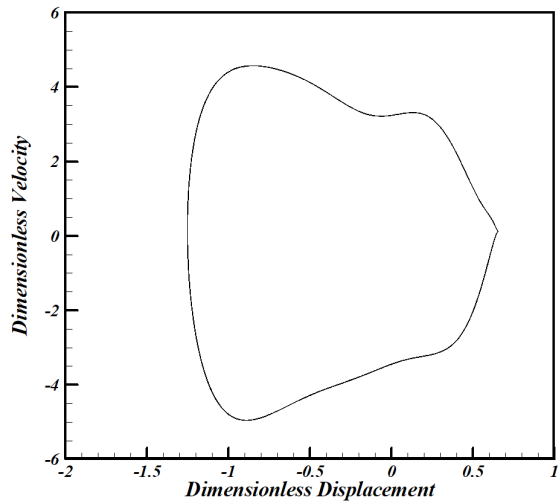
Fig. 10. Nonlinear flutter response ($n=1, \lambda=380, R_x=R_y=5.5\pi^2, M=2$). (a) Non-dimensional deflection, (b) phase diagram, (c) frequency spectrum

The effect of the Mach number on the aforementioned aerothermoelastic stability margins of the plate with $n=1$ is shown in Fig. 9. It can be seen that most changes occur at the common boundary of the chaotic and LCO regions. Thus, the increase of Mach number causes the chaotic region to extend toward the LCO region while these changes are not considerable at the other boundaries.

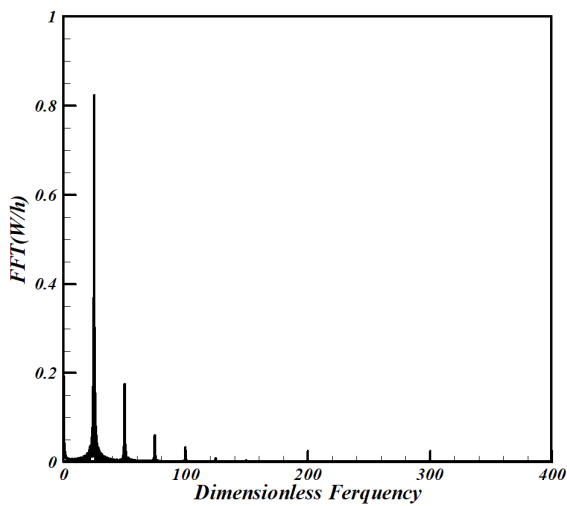
Time history response and the related phase diagram and frequency spectrum diagram at a specified condition ($n=1, R_x=R_y=5.5\pi^2, \lambda=380$) are shown in Figs. 10 to 12. The limit cycle with simple harmonic motion of plate under airflow with the Mach number $M=2$ is depicted in Fig. 10. As the Mach number increases ($M=5$), the simple harmonic motion remains periodic but not simple harmonic, as shown in Fig. 11. If the Mach number increases again ($M=8$), the periodic motion becomes a chaotic motion, as shown in Fig. 12. This figure can explain the extension of the chaotic region in Fig. 9. As it is evident, as the Mach number increases the envelope of the frequency spectrum covers more frequencies and reveals the occurrence of a chaotic behavior in the aeroelastic system.



(a)

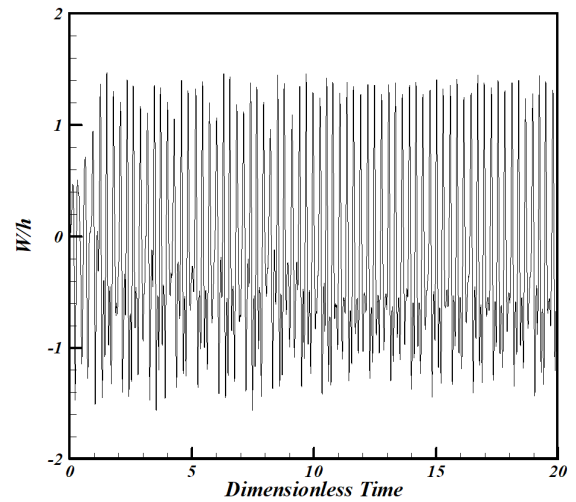


(b)

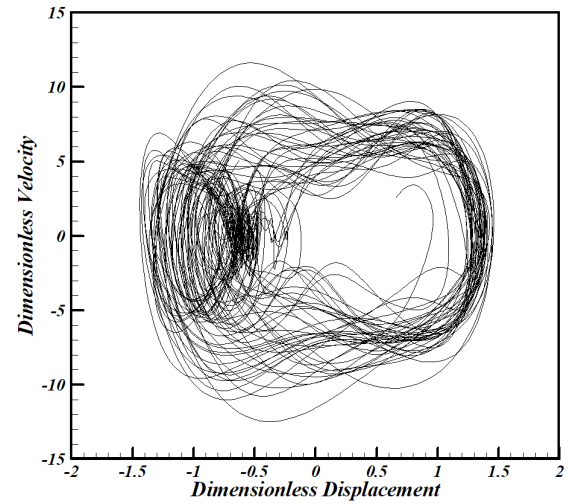


(c)

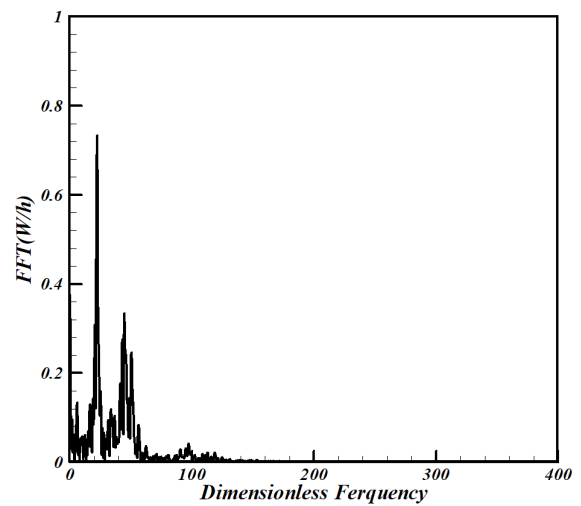
Fig. 11. Nonlinear flutter response ($n=1, \lambda=380, R_x=R_y=5.5\pi^2, M=5$). (a) Non-dimensional deflection, (b) phase diagram, (c) frequency spectrum



(a)



(b)



(c)

Fig. 12. Nonlinear flutter response ($n=1, \lambda=380, R_x=R_y=5.5\pi^2, M=8$). (a) Non-dimensional deflection, (b) phase diagram, (c) frequency spectrum

5- Conclusions

In this study, the GDQM has been used to obtain the ordinary differential form of the aerothermoelastic equations of a FG flat plate in hypersonic regime. To investigate the aerothermoelastic behavior of the plate, the 4th order Runge-Kutta numerical method has been utilized. The evaluation of the obtained results in comparison with those available in literature shows the fidelity and ability of the GDQM to study the aerothermoelastic behavior of a FG panel in hypersonic regime. However, it should be noted that the application of this method is much simpler than other well-known methods such as (Galerkin, FEM). Also, it was found that the nonlinear panel flutter analysis with GDQM is extremely sensitive to the grid point distribution. So, the well-known Chebyshev-Gauss-Lobatto distribution is not suitable for this type of problems, but Tomasiello's distribution [46] can be used as an efficient and suitable choice.

The obtained results showed that the using of physical neutral surface concept in the derivation of the aeroelastic governing equations led the same results for the response of a FG panel which uses mid-surface based formulation in conjunction with thin plate theory. Finally, this study reveals that increasing of the surface temperature of a FG plate leads to decrease in critical dynamic pressure due to the reduction of structural Rigidity. The results showed that the increase of Mach number has little effect on the flutter onset velocity. In addition, it was shown that when a FG plate is exposed to supersonic airflow, the use of linear and nonlinear aerodynamic piston theories does not make much difference. But with Mach number increasing toward hypersonic flow, this difference becomes significant. Also, the increase of Mach number can cause the chaotic region to expand the flutter (LCO) region in the stability margins diagram. Also, in-plane thermal load, thickness ratio, and surface temperature (Tc) were found to have significant effects on the critical dynamic pressure and stability margins of a FG plate.

Appendix A

The C_i coefficients in Eq. (39) are defined through the following relations:

$$C_1 = A_{ik}^{(4)x} - \frac{A_{i,2}^{(4)x} .AXK 1 + A_{i,N-1}^{(4)x} .AXKN}{AXN}$$

$$C_2 = (A_{ik1}^{(2)x} - \frac{A_{i,2}^{(2)x} .AXK 1 + A_{i,N-1}^{(2)x} .AXKN}{AXN}) \times (A_{jk2}^{(2)y} - \frac{A_{j,2}^{(2)y} .AYK 1 + A_{j,M-1}^{(2)y} .AYKM}{AYM})$$

$$C_3 = (A_{jk}^{(4)y} - \frac{A_{j,2}^{(4)y} .AYK 1 + A_{j,M-1}^{(4)y} .AYKM}{AYM})$$

$$C_4 = c_k c_p (A_{kn}^{(1)x} - \frac{A_{k,2}^{(1)x} .AXK 1 + A_{k,N-1}^{(1)x} .AXKN}{AXN}) \times (A_{pm}^{(1)x} - \frac{A_{p,2}^{(1)x} .AXK 1 + A_{p,N-1}^{(1)x} .AXKN}{AXN}) \times (A_{il}^{(2)x} - \frac{A_{i,2}^{(2)x} .AXK 1 + A_{i,N-1}^{(2)x} .AXKN}{AXN})$$

$$C_5 = c_k c_p (A_{kq}^{(1)y} - \frac{A_{k,2}^{(1)y} .AYK 1 + A_{k,M-1}^{(1)y} .AYKM}{AYM}) \times (A_{ps}^{(1)y} - \frac{A_{p,2}^{(1)y} .AYK 1 + A_{p,M-1}^{(1)y} .AYKM}{AYM}) \times (A_{il}^{(2)x} - \frac{A_{i,2}^{(2)x} .AXK 1 + A_{i,N-1}^{(2)x} .AXKN}{AXN})$$

$$C_6 = c_k c_p (A_{kn}^{(2)x} - \frac{A_{k,2}^{(2)x} .AXK 1 + A_{k,N-1}^{(2)x} .AXKN}{AXN}) \times (A_{il}^{(2)x} - \frac{A_{i,2}^{(2)x} .AXK 1 + A_{i,N-1}^{(2)x} .AXKN}{AXN})$$

$$C_7 = c_k c_p (A_{pq}^{(2)y} - \frac{A_{p,2}^{(2)y} .AYK 1 + A_{p,M-1}^{(2)y} .AYKM}{AYM}) \times (A_{il}^{(2)x} - \frac{A_{i,2}^{(2)x} .AXK 1 + A_{i,N-1}^{(2)x} .AXKN}{AXN})$$

$$C_8 = c_k c_p (A_{kn}^{(1)x} - \frac{A_{k,2}^{(1)x} .AXK 1 + A_{k,N-1}^{(1)x} .AXKN}{AXN}) \times (A_{pq}^{(1)y} - \frac{A_{p,2}^{(1)y} .AYK 1 + A_{p,M-1}^{(1)y} .AYKM}{AYM}) \times (A_{ik1}^{(1)x} - \frac{A_{i,2}^{(1)x} .AXK 1 + A_{i,N-1}^{(1)x} .AXKN}{AXN}) \times (A_{jk2}^{(1)y} - \frac{A_{j,2}^{(1)y} .AYK 1 + A_{j,M-1}^{(1)y} .AYKM}{AYM})$$

$$C_9 = c_k c_p (A_{ks}^{(1)x} - \frac{A_{k,2}^{(1)x} .AXK 1 + A_{k,N-1}^{(1)x} .AXKN}{AXN}) \times (A_{pt}^{(1)y} - \frac{A_{p,2}^{(1)y} .AYK 1 + A_{p,M-1}^{(1)y} .AYKM}{AYM}) \times (A_{ik1}^{(1)x} - \frac{A_{i,2}^{(1)x} .AXK 1 + A_{i,N-1}^{(1)x} .AXKN}{AXN}) \times (A_{jk2}^{(1)y} - \frac{A_{j,2}^{(1)y} .AYK 1 + A_{j,M-1}^{(1)y} .AYKM}{AYM})$$

$$C_{10} = c_k c_p \left(A_{ks}^{(1)x} - \frac{A_{k,2}^{(1)x} \cdot AXK1 + A_{k,N-1}^{(1)x} \cdot AXKN}{AXN} \right) \\ \times \left(A_{pt}^{(1)x} - \frac{A_{p,2}^{(1)x} \cdot AXK1 + A_{p,N-1}^{(1)x} \cdot AXKN}{AXN} \right) \\ \times \left(A_{jq}^{(1)y} - \frac{A_{j,2}^{(1)y} \cdot AYK1 + A_{j,M-1}^{(1)y} \cdot AYKM}{AYM} \right)$$

$$C_{11} = c_k c_p \left(A_{pm}^{(1)y} - \frac{A_{p,2}^{(1)y} \cdot AYK1 + A_{p,M-1}^{(1)y} \cdot AYKM}{AYM} \right) \\ \times \left(A_{kn}^{(1)y} - \frac{A_{k,2}^{(1)y} \cdot AYK1 + A_{k,M-1}^{(1)y} \cdot AYKM}{AYM} \right) \\ \times \left(A_{jq}^{(2)y} - \frac{A_{j,2}^{(2)y} \cdot AYK1 + A_{j,M-1}^{(2)y} \cdot AYKM}{AYM} \right)$$

$$C_{12} = c_k c_p \left(A_{pt}^{(2)x} - \frac{A_{p,2}^{(2)x} \cdot AXK1 + A_{p,N-1}^{(2)x} \cdot AXKN}{AXN} \right) \\ \times \left(A_{jq}^{(2)y} - \frac{A_{j,2}^{(2)y} \cdot AYK1 + A_{j,M-1}^{(2)y} \cdot AYKM}{AYM} \right)$$

$$C_{13} = c_k c_p \left(A_{kn}^{(2)y} - \frac{A_{k,2}^{(2)y} \cdot AYK1 + A_{k,M-1}^{(2)y} \cdot AYKM}{AYM} \right) \\ \times \left(A_{jq}^{(2)y} - \frac{A_{j,2}^{(2)y} \cdot AYK1 + A_{j,M-1}^{(2)y} \cdot AYKM}{AYM} \right)$$

$$C_{14} = \left(A_{ik}^{(2)x} - \frac{A_{i,2}^{(2)x} \cdot AXK1 + A_{i,N-1}^{(2)x} \cdot AXKN}{AXN} \right)$$

$$C_{15} = \left(A_{jk}^{(2)y} - \frac{A_{j,2}^{(2)y} \cdot AYK1 + A_{j,M-1}^{(2)y} \cdot AYKM}{AYM} \right)$$

$$C_{16} = \left(A_{ik}^{(1)x} - \frac{A_{i,2}^{(1)x} \cdot AXK1 + A_{i,N-1}^{(1)x} \cdot AXKN}{AXN} \right)$$

where

$$AXN = A_{N,2}^{(2)x} \cdot A_{1,N-1}^{(2)x} - A_{1,2}^{(2)x} \cdot A_{N,N-1}^{(2)x}$$

$$AXK1 = A_{1,k}^{(2)x} \cdot A_{N,N-1}^{(2)x} - A_{1,N-1}^{(2)x} \cdot A_{N,k}^{(2)x}$$

$$AXKN = A_{1,2}^{(2)x} \cdot A_{N,k}^{(2)x} - A_{1,k}^{(2)x} \cdot A_{N,2}^{(2)x}$$

$$AYN = A_{M,2}^{(2)y} \cdot A_{1,M-1}^{(2)y} - A_{1,2}^{(2)y} \cdot A_{M,M-1}^{(2)y}$$

$$AYK1 = A_{1,k}^{(2)y} \cdot A_{M,M-1}^{(2)y} - A_{1,M-1}^{(2)y} \cdot A_{M,k}^{(2)y}$$

$$AYKN = A_{1,2}^{(2)y} \cdot A_{M,k}^{(2)y} - A_{1,k}^{(2)y} \cdot A_{M,2}^{(2)y}$$

References

- [1] Y. Miyamoto, W.A. Kaysser, B.H. Rabin, A. Kawasaki, R.G. Ford, *Functionally Graded Materials: Design, Processing and Applications*, Kluwer Academic Publisher, Boston, MA, 1999.
- [2] J.C. Houbolt, *A study of several aerothermoelastic problems of aircraft structures in high-speed flight*, ETH Zurich, 1958.
- [3] V.V. Bolotin, *Nonconservative problems of the theory of elastic stability*, Macmillan, 1963.
- [4] E.H. Dowell, Nonlinear oscillations of a fluttering plate, *AIAA Journal*, 4(7) (1966) 1267–1275.
- [5] E.H. Dowell, *Aeroelasticity of Plates and Shells*, Noordhoff, in, Leyden, 1975.
- [6] H.G. Schaeffer, W. L. Heard, Flutter of a flat panel subjected to nonlinear temperature distribution, *AIAA Journal*, 30(10) (1965) 1918-1923.
- [7] S.G. McIntosh, *Theoretical considerations of some nonlinear aspects of hypersonic panel flutter*, Final Report, NASA Grant NG, 05-020-102, Department of Aeronautics and Astronautics, Stanford University, Stanford, CA, 1970.
- [8] S.C. McIntosh, Effect of hypersonic nonlinear aerodynamic loading on panel flutter, *AIAA Journal*, 11(1) (1973) 29-32.
- [9] F.E. Eastep, S.C. McIntosh, Analysis of nonlinear panel flutter and response under random excitation or nonlinear aerodynamic loading, *AIAA Journal*, 9(3) (1971) 411-418.
- [10] D.Y. Xue, C. Mei, Finite element nonlinear panel flutter with arbitrary temperatures in supersonic flow, *AIAA Journal*, 31(1) (1993) 154–62.
- [11] D.Y. Xue, C. Mei, Finite element nonlinear flutter and fatigue life of two-dimensional panels with temperature effects, *Journal of Aircraft*, 30(6) (1993) 993-1000.
- [12] T. Bein, P. Friedmann, X. Zhong, I. Nydick, Hypersonic flutter of a curved shallow panel with aerodynamic heating, *AIAA Journal*, (1993) 93-1318
- [13] G. Cheng, C. Mei, Finite Element Modal Formulation for Hypersonic Panel Flutter Analysis with Thermal Effects, *AIAA Journal*, 42(4) (2004) 687-695.
- [14] S.H. Pourtakdoust, S.A. Fazelzadeh, Nonlinear Aerothermoelastic Behavior of Skin Panel with Wall Shear Stress Effect, *Journal of Thermal Stresses*, 28 (2005) 147-169.

- [15] A.J. Culler, J.J. McNamara, Studies on fluid–thermal–structural coupling for aerothermoelasticity in hypersonic flow, *AIAA Journal*, 48(8) (2010) 1721-1738.
- [16] A.J. Culler, J.J. McNamara, Impact of fluid-thermal-structural coupling on response prediction of hypersonic skin panels, *AIAA Journal*, 49(11) (2011) 2393-2406.
- [17] P. Prakash, M. Ganapathi, Supersonic flutter characteristics of functionally graded flat panels Including thermal effects, *Composite Structures*, 13 (2006) 257-264.
- [18] H.-S. Shen, Thermal post-buckling behavior of shear deformable FGM plates with temperature-dependent properties, *International Journal of Mechanical Sciences*, 49(4) (2007) 466-478.
- [19] K.-J. Sohn, J.-H. Kim, Structural stability of functionally graded panels subjected to aero-thermal loads, *Composite Structures*, 82 (2008) 317-25.
- [20] K.-J. Sohn, J.-H. Kim, Nonlinear thermal flutter of functionally graded panels under a supersonic flow, *Composite Structure*, 88 (2009) 380-87.
- [21] S. A. Fazelzadeh, M. Hosseini, H. Madani, Thermal Divergence of Supersonic Functionally Graded Plates, *Journal of Thermal Stresses*, 34 (8) (2011) 759-777.
- [22] M. Hoseini, S. A. Fazelzadeh, P. Marzocca, Chaotic and Bifurcation Dynamic Behavior of Functionally Graded Curved Panels Under Aero-Thermal Loads, *IJBC-D International Journal of Bifurcation and Chaos*, 21 (2011) 931-954.
- [23] P. Marzocca, S.A. Fazelzadeh, M. Hosseini, A review of nonlinear aero-thermo-elasticity of functionally graded panels, *Journal of Thermal Stresses*, 34 (5 & 6) (2011) 536-568.
- [24] H.M. Navazi, H. Haddadpour, Nonlinear aerothermoelastic analysis of homogeneous and functionally graded plates in supersonic airflow using coupled models, *Composite Structures*, 93 (2011) 2554-65.
- [25] A.H. Sofiyev, Buckling analysis of freely-supported functionally graded truncated conical shells under external pressures, *Composite Structures*, (132) (2015) 746-758.
- [26] A.H. Sofiyev, On the vibration and stability of shear deformable FGM truncated conical shells subjected to an axial load, *Composites Part B Engineering*, (80) (2015) 53-62.
- [27] M.R. Amoozgar, H. Shahverdi, Analysis of nonlinear fully intrinsic equations of geometrically exact beams using generalized differential quadrature method, *Acta Mech*, 227(5) (2016) 1265-1277.
- [28] R.E. Bellman, J. Casti, Differential quadrature and long-term integration, *Journal of Mathematical Analysis and Applications*, 34 (1971) 235-238.
- [29] C.W. Bert, S.K. Jang, A.G. Striz, Two new approximate methods for analyzing free vibration of structural components, *AIAA Journal*, 26 (1988) 612-618.
- [30] C.W. Bert, M. Malik, Differential quadrature in computational mechanics: a review, *Applied mechanics reviews*, 49 (1996) 1-27.
- [31] C.W. Bert, S.K. Jang, A.G. Striz, Nonlinear bending analysis of orthotropic rectangular plates by the method of differential quadrature, *Computational Mechanics*, 5 (1989) 217-226.
- [32] C. Shu, B.E. Richards, Application of generalized differential quadrature to solve two-dimensional incompressible Navier-Stokes equations, *International Journal for Numerical Methods in Fluids*, 15 (1992) 791-798.
- [33] C. Shu, C.M. Wang, Treatment of mixed and non-uniform boundary conditions in GDQ vibration analysis of rectangular plate, *Engineering structures*, 21 (1999) 125-134.
- [34] S.A. Fazelzadeh, P. Malekzadeh, P. Zahedinejad, M. Hosseini, Vibration analysis of functionally graded thin-walled rotating blades under high-temperature supersonic gas flow using the DQM, *Journal of Sound and Vibration*, 306 (2007) 333–348.
- [35] F. Tornabene, A. Liverani, G. Caligiana, FGM and laminated doubly curved shells and panels of revolution with a free-form meridian: A 2-D GDQ solution for free vibrations, *International Journal of Mechanical Sciences*, 53(6) (2011) 446-470.
- [36] F. Tornabene, N. Fantuzzi, M. Baccocchi, The local GDQ method applied to general higher-order theories of doubly-curved laminated composite Shells and Panels: the Free Vibration Analysis, *Composite Structures*, 116(1) (2014) 637-660.
- [37] F. Tornabene, N. Fantuzzi, E. Viola, R.C. Batra, Stress and strain recovery for functionally graded free-form and doubly-curved sandwich shells using higher-order equivalent single layer theory, *Composite Structures*, 119(1) (2015) 67-89.
- [38] N. Fantuzzi, F. Tornabene, E. Viola, Four-parameter functionally graded cracked plates of arbitrary shape: A GDQFEM solution for free vibrations, *Mechanics of Advanced Materials and Structures*, 23 (2016) 89-107
- [39] F. Tornabene, N. Fantuzzi, F. Ubertini, E. Viola, Strong formulation finite element method based on differential quadrature: A survey, *Applied Mechanics Reviews*, 67(2) (2015) 1-55.
- [40] H. Shahverdi, V. Khalafi, S. Noori, Aerothermoelastic analysis of functionally graded plates using generalized differential quadrature method, *Latin American Journal of Solids and Structures*, 13 (2016) 797-819
- [41] H. Shahverdi, V. Khalafi, 2016. Bifurcation analysis of FG curved panels under simultaneous aerodynamic and thermal loads in hypersonic flow, *Composite Structures*, 146 (2016) 84-94.
- [42] B.A. Miller, J.J. McNamara, S.M. Spottswood, A.J. Culler, The impact of flow induced loads on snap-through behavior of acoustically excited, thermally buckled panels, *Journal of Sound and Vibration*, 330 (2011) 5736-5752.
- [43] D.-G. Zhang, Y.-H. Zhou, A theoretical analysis of FGM thin plates based on physical neutral surface, *Computational Material Science*, 44 (2008) 716-720.
- [44] D.-G. Zhang, Nonlinear bending analysis of FGM beams based on physical neutral surface and high order shear deformation theory, *Composite Structures*, 100

(2013) 121-126.

[45] C. Shu, *Differential Quadrature and Its application in engineering*, Springer-Verlag London Limited, London, 2000.

[46] S. Tomasiello, Differential quadrature method: Application to Initial-Boundary-Value Problems, *Journal of Sound and Vibration*, 218(4) (1998) 573-585.

Please cite this article using:

V. Khalafi, H. Shahverdi, S. Noori, Nonlinear Aerothermoelastic Analysis of Functionally Graded Rectangular Plates

Subjected to Hypersonic Airflow Loadings, *AUT J. Mech. Eng.*, 2(2) (2018) 217-232.

DOI: 10.22060/ajme.2018.12712.5407



